A LAGRANGIAN REACTION-DIFFUSION MODEL FOR PREDICTING THE IGNITABILITY OF PRESSURIZED HYDROGEN RELEASES

Maxwell, B.M.[1] and Radulescu, M.I.[1]
[1] Department of Mechanical Engineering, University of Ottawa, 161 Louis Pasteur, Ottawa, K1N 6N5, Canada, maxwellbrian@yahoo.ca

ABSTRACT

Previous experiments demonstrated that the accidental release of high pressure hydrogen into air can lead to the possibility of spontaneous ignition. It is believed that this ignition is due to the heating of the mixing layer, between hydrogen and air, that is caused by the shock wave driven by the pressurized hydrogen during the release. Currently, this problem is poorly understood and not amenable to direct numerical simulation. This is due to the presence of a wide range of scales between the sizes of the blast wave driven and the very thin mixing layer. The present study addresses this fundamental ignition problem and develops a solution framework in order to predict the ignition event for given hydrogen storage pressures and dimension of the release hole. In this problem, only the mixing layer between the hydrogen and air is considered. This permits us to use much higher resolution than previous studies. This mixing layer, at the jet head, is advected as a Lagrangian fluid particle. The key physical processes in the problem are identified to be the mixing of the two gases at the mixing layer, the initial heating by the shock wave, and a cooling effect due to the expansion of the mixing layer. The results of the simulations indicate that for every storage pressure, there exists a critical hole size below which ignition is prevented during the release process. Close inspection of the results indicate that this limit is due to the competition between the heating provided by the shock wave and the cooling due to expansion. Furthermore, the results also indicate that the details of the mixing process do not play a significant role to leading order. The limiting ignition criteria were found to be well approximated by the Homogeneous Ignition Model of Cuenot and Poinsot, supplemented by a heat loss term due to expansion. Therefore, turbulent mixing occurring in reality is not likely to affect the ignition limits derived in the present study. Comparison with existing experiments showed very good agreement.

1.0 INTRODUCTION

Hydrogen gas is currently a clean alternative to using gasoline or other fuels in automobiles. It can be used in internal combustion engines or in fuel cells to generate power. However, a primary concern with using hydrogen is the safety of storing and handling the fuel. In order for hydrogen to be used as a fuel, it must be compressed to high pressures. This ensures that the fuel has a large amount of energy available in a small volume. Unfortunately, the accidental release of high pressure hydrogen into air can lead to spontaneous ignition, without a spark or flame present. It is believed that this ignition is due to the shock induced heating of the mixing layer, between hydrogen and air.

During the release of high pressure hydrogen into air a shock wave is formed. This shock wave travels through the air heating it up to high temperature and pressure. It has previously been postulated that the high temperature induced by the shock wave can trigger ignition in regions behind the shock where the gases have mixed. In particular, this diffusion ignition has been observed experimentally by various groups [1, 2, 3, 4] within tubes at constant pressure. However, in addition to this shock induced heating during release, the gas is also expanded and cooled. This is especially evident in the absence of a tube. Therefore, there are actually two competing mechanisms that control ignition; one of heat addition due to chemical reactions in the shocked gas, and one of cooling due to expansion. The present study addresses this fundamental ignition problem and develops a solution framework in order to predict the ignition event for given hydrogen storage pressures and dimension of the release hole.

At present, this problem is poorly understood and not amenable to direct numerical simulation. Current CFD codes [5, 6] for the hydrogen release problem, which take expansion into account, lack the resolution necessary to capture the ignition phenomena that occurs at small scales within the mixing layer. The size of the mixing layer is very small compared to the size of the blast wave itself and is not resolved in these codes. In this study, only the mixing layer between the hydrogen and air is considered. This permits us to use much higher resolution than previous studies. This mixing layer, at the jet head, is advected as a Lagrangian fluid particle. The evolution of its thermo-chemical structure can thus be readily obtained. The key physical processes in the problem are identified to be the mixing of the two gases at the mixing layer, the initial heating by the shock wave, and a cooling effect due to the expansion of the mixing layer. Specifically, the shock induced heating is evaluated by solving the shock tube problem in terms of the initial storage pressure ratio. This provides the initial conditions at the mixing layer. The chemical reactions at the mixing layer are computed using Dryer's chemical kinetic mechanism [11], in order to capture high pressure reactions. The molecular mixing process is solved exactly using the mixture average transport properties of each chemical specie. The expansion process of the hydrogen jet is solved separately using a compressible flow solver for non-reacting releases. Finally, an approximate model that reacts a pre-determined, highly reactive, mixture of fuel and air up to the point of ignition is also developed using the *homogenous mixing ignition* (HMI) method [14] in order to study the significance of mixing in the hydrogen ignition problem.

2.0 GOVERNING EQUATIONS AND NUMERICAL MODELS

2.1 Governing Equations for the Hydrogen Release Problem

The reaction-diffusion-expansion phenomenon, following a bounded one-dimensional domain, which encompasses the turbulent mixing layer at the head of the jet, is governed by the conservation of energy and the conservation of mass of each chemical specie within the fluid particle. These equations are given below in (1) and (2) in one dimensional Lagrangian coordinates. Lagrangian coordinates were chosen since it is useful for keeping track of the gas as it gas expands and occupies more space. The mixing layer at the head of the jet is shown in Figure 1 and is labeled *Area of Interest*. The figure is a two-dimensional image of the jet release generated from Amrita [7] using a non-reactive compressible flow solver.

Figure 1.
The figure to the right represents the temperature profile during a non-reactive release of hydrogen into the atmosphere. Lighter colours represent higher temperatures. The numerical simulation was run using the AMRITA language [7] to solve the Euler equations at a resolution of 512 grid points across the orifice. The initial pressure of the tank in this figure is 300 atmospheres.

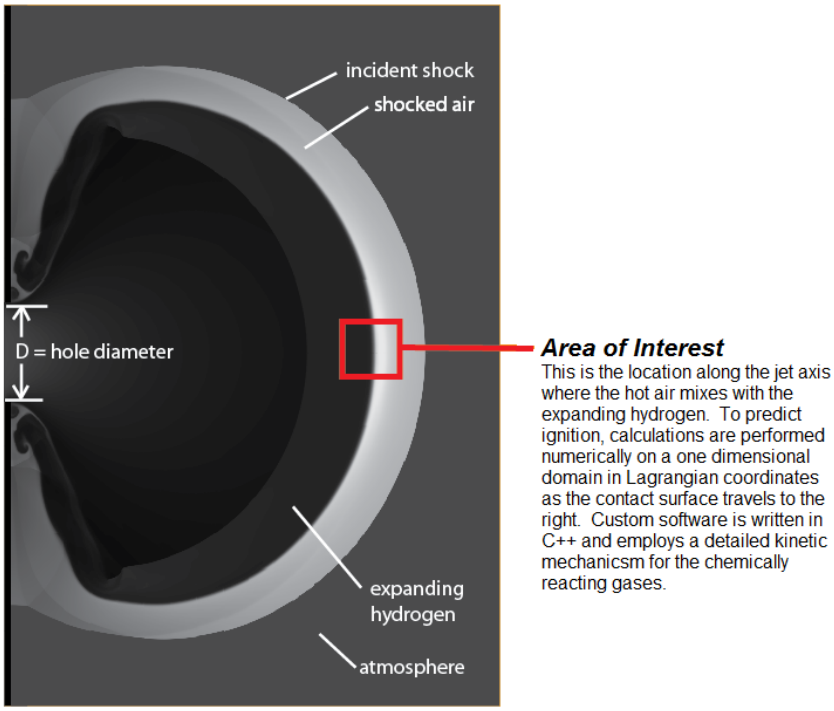

Conservation of mass of the ith specie:

$$\rho \frac{\partial Y_i}{\partial t} = \omega_i - \rho \frac{\partial (\rho Y_i v_{d,i})}{\partial m}, \quad (1)$$

Conservation of energy:

$$\rho C_p \frac{\partial T}{\partial \mathrm{t}} = \frac{\partial P}{\partial \mathrm{t}} - \sum_{i=1}^{N} h_i \omega_i + \rho \frac{\partial}{\partial m}\left(\mathrm{k}\rho \frac{\partial \mathrm{T}}{\partial \mathrm{m}}\right) - \rho^2 \frac{\partial \mathrm{T}}{\partial \mathrm{m}} \sum_{i=1}^{N} Y_i C_{p,i} v_{d,i}, \quad (2)$$

where T, P, ρ, C_p, k, h_i, Y_i, and $v_{d,i}$, is the temperature, pressure, density, specific heat, thermal conductivity, enthalpy of specie i, mass fraction of specie i, and diffusional velocity of specie i, respectively. The rate of change of density for specie i per unit time for a fluid particle, $\rho \frac{\partial Y_i}{\partial t}$, is controlled by; 1) the net rate of production of specie i within the fluid particle, ω_i, and 2) the diffusion of specie i to neighbouring particles, $\frac{\rho}{x^\alpha} \frac{\partial (x^\alpha \rho Y_i v_{d,i})}{\partial m}$. Similarly, the rate of change of energy per unit time for a fluid particle, $\rho C_p \frac{\partial T}{\partial \mathrm{t}}$, is controlled by; 1) the rate of change of pressure (expansion), $\frac{\partial P}{\partial \mathrm{z}}$, of the fluid particle, 2) energy addition due to the reaction of N species, $\sum_{i=1}^{N} h_i \omega_i$, 3) the diffusion of heat to neighbouring particles, $\rho \frac{\partial}{\partial m}\left(\mathrm{k}\rho x^\alpha \frac{\partial \mathrm{T}}{\partial \mathrm{m}}\right)$, and 4) the energy addition due to differences in diffusional velocities of the species and temperature gradients within the fluid particle, $\rho^2 x^\alpha \frac{\partial \mathrm{T}}{\partial \mathrm{m}} \sum_{i=1}^{N} Y_i C_{p,i} v_{d,i}$. The Lagrangian coordinate, m, can be converted to the Eularian coordinate, x, through the following transformation:

$$m(x,t) = \int_{x_o}^{x} \rho(x,t) x^\alpha dx, \quad (3)$$

The above equations have been derived in Lagrangian coordinates using the approach taken by [8]. A similar derivation for a control volume in Eularian coordinates can be found in [9]. To arrive at equations (1) and (2) the following approximations were made: 1) Dufour and Soret effects are neglected, 2) Radiation effects are neglected, 3) Viscous dissipation is neglected, 4) external body forces acting on the mass particle are neglected, and 4) A low mach number for the velocity of the jet is assumed, thus pressure gradients are neglected across the contact surface.

2.2 Expansion Rate

Radulescu and Law [17] have previously determined the scaling parameters for under-expanded non-reactive hydrogen jets using a compressible flow solver for non-reacting releases. In their non-dimensional analysis, the pressure-time history at the interface between the gasses for different jet conditions was found to be well approximated by a unique relation. The rate at which the pressure at the interface decays in terms of a non-dimensional time scaling parameter, τ, is shown in Figure 3. This scaling parameter was found to depend on the discharge flow rate, and hence the size of the hole through which the gas escapes as well as the chocked velocity at the hole. The unique relation describing the pressure at the interface, regardless of the initial pressure ratio $\frac{p_{Ao}}{p_{Bo}}$, in terms of τ is found to be:

$$\frac{p_i}{p_{Bo}} = 12.2\tau^{-0.68}, \quad (13)$$

where the scaling parameter

$$\tau = \left(\frac{\rho_{Bo}}{\rho_{Ao}}\left(\frac{2}{\gamma_A+1}\right)^{-1/(\gamma_A-1)}\right)^{1/j} \frac{t a_{Ao}}{R\Lambda}\left(\frac{2}{\gamma_A+1}\right)^{1/2}, \quad (14)$$

p_i is the pressure at the contact surface, a is the speed of sound, γ_A is the ratio of specific heats for the stored hydrogen , t is time, and R is the radius of the hole. j and Λ are constants whose values are equal to 2 and 1.2 respectively [17].

Furthermore, at the onset of release there is initially a period where the pressure at the interface remains constant. This can clearly be seen for the case where $\frac{p_{Ao}}{p_{Bo}} = 88$ in Figure 1. The reason for this initial period of constant pressure is due to the time required for information regarding expansion at the corner of the hole to reach the location of the particle along the axis of the jet. To account for this delay, the value of τ is calculated for when $\frac{p_i}{p_{Bo}}$ is equal to the initial condition found from the shock tube solution. The simulations are then started at time zero of the release process, incorporating this period of constant pressure.

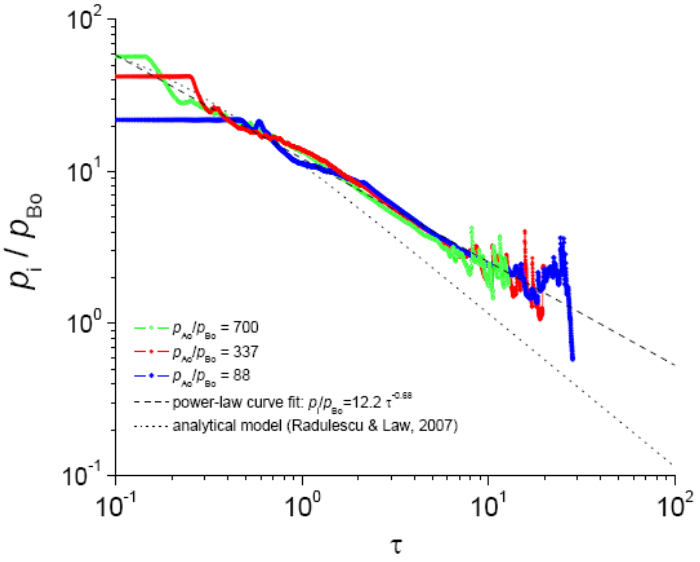

Figure 3. Evolution of the contact surface pressure along the jet axis for round jets obtained numerically for various storage pressure to ambient pressure ratios from Radulescu and Law, 2007 [17].

2.3 Numerical Method for Lagrangian Reaction-Diffusion Model

Equations (1) and (2) are integrated numerically using an operator splitting technique which solves the diffusion, reaction, and source terms separately over one time step. Each operation is solved explicitly based on information known from the previous operation. The thermodynamic and transport properties are evaluated at each operation using the Cantera [10] libraries for C++. The kinetic mechanism used was developed by [11] and is specifically designed for hydrogen chemistry. Finally the Sundials CVODE [12] integrator is used to handle the stiff chemistry of the reaction terms.

For operator splitting, equations (1) and (2) are split up and solved independently across the given time step. The steps are explained below.

Step 1: Diffusion Step

First the diffusive terms are solved over one whole time step. The equations that are solved for planar geometry in this step are:

$$\rho \frac{\partial Y_i}{\partial t} = -\rho \frac{\partial (\rho Y_i v_{d,i})}{\partial m}, \tag{4}$$

$$\rho C_p \frac{\partial T}{\partial \mathrm{t}} = \rho \frac{\partial}{\partial m}\left(\mathrm{k}\rho \frac{\partial \mathrm{T}}{\partial \mathrm{m}}\right) - \sum_{i=1}^{N} \rho^2 Y_i C_{p,i} v_{d,i} \frac{\partial \mathrm{T}}{\partial \mathrm{m}}, \tag{5}$$

Equations (4) and (5) are discritized using central difference approximations on the diffusive terms and explicit time stepping for the unsteady terms. The diffusion velocities, $v_{d,i}$, are evaluated using the mixture-averaged formulas found in [13]. These formulas, however, are given in Eularian coordinates. Therefore, they must be transformed to Lagrangian coordinates using the transformation in equation (3). The diffusion velocities for each species can be computed in Lagrangian coordinates using the formula in equation (6).

$$v_{d,i} = \rho \left[-\frac{1}{X_i} D_{im} \frac{\partial X_i}{\partial m} + \sum_{j=1}^{N} \frac{Y_j}{X_j} D_{jm} \frac{\partial X_j}{\partial m} \right], \tag{6}$$

where X_i is the mole fraction of specie i and D_{im} is the mixture-averaged diffusion coefficient of specie i.

Step 2: Reaction Step

Once the solution field is updated from step 1, the reaction terms are then solved over the same time step using the Sundials CVODE integrator. The equations solved for this step are:

$$\rho \frac{\partial Y_i}{\partial t} = \omega_i, \tag{7}$$

$$\rho C_p \frac{\partial T}{\partial \mathrm{t}} = -\sum_{i=1}^{N} h_i \omega_i, \tag{8}$$

Step 3: Source Term Step

The expansion term, $\frac{\partial P}{\partial \mathrm{t}}$, in the energy equation (2) is treated as a source term and is evaluated independently of the other terms. Once the solution field is updated from the previous step, the pressure is updated and the following equation is solved over the same time step:

$$\rho C_p \frac{\partial T}{\partial \mathrm{t}} = \frac{\partial P}{\partial \mathrm{t}}, \tag{9}$$

2.4 Approximate Homogeneous Mixing Ignition Model

To simplify the problem, the ignition phenomenon is also modeled using the *homogenous mixing ignition* (HMI) method described in [14]. Transport effects are implicitly taken into account by considering the ignition time history of a representative fixed mixture fraction of fuel and air. The most reactive mixture fraction is considered, since this is where the first ignition site would occur. This approximation is made by considering the activation energy asymptotics of ignition-diffusion problems where heat and mass diffuse at the same rate. Also, the approximation assumes that heat release plays a minor role prior to the ignition event. This approach has been shown to be a good approximation for predicting non-premixed hydrogen air ignition problems [14]. The resulting governing equations that are solved numerically for the approximate model are reduced to:

$$\rho \frac{\partial Y_i}{\partial t} = \omega_i, \tag{10}$$

$$\rho C_p \frac{\partial T}{\partial \mathrm{t}} = \frac{\partial P}{\partial \mathrm{t}} - \sum_{i=1}^{N} h_i \omega_i, \tag{11}$$

2.5 Initial and Boundary Conditions

To determine the initial boundary conditions of the problem, the properties of the hot air and cold fuel on each side of the contact surface are found by solving the well known shock tube problem described in [15]. In this case, however, the shock tube problem is solved by taking realistic thermal properties into account. The solutions across the shock discontinuity and expansion fan are found using the numerical methods described in [16] and iterated until the pressure and velocity at the contact surface

are matched. Once the boundaries are known for the *Lagrangian reaction-diffusion model*, the domain is then filled with the gasses. Each half of the domain contains each gas. However, rather than separate the two gases by a discontinuity, a smoothing function is applied across 6 grid points to avoid computational difficulties that may arise from computing infinite gradients. This approach was used by [14] and the smoothing function is given by equation (12).

$$z = \frac{1}{2}\left[1 + \text{erf}\left(\frac{m-m_o}{d}\right)\right], \tag{12}$$

where, z is the mixture fraction, or mass fraction, of the fuel in the mixture and is defined in [14] (z=0 for pure air and z=1 for pure fuel), m is the Largrangian coordinate, m_o is the midpoint in the domain, and d is the number of grid points across which the smoothing function is applied (d=6 in this case). The pressure of the ambient air is taken to be 1 atm and the initial temperatures of both gasses are taken to be 300K.

For the simplified *homogeneous mixing ignition* model, the most reactive mixture fraction, z, between the hot air and cold hydrogen is found by reacting various mixtures of the two gases, computed from the above shock tube solution, until the mixture with the smallest ignition delay is found. Ignition delay times for various mixtures of hot air and cold hydrogen are shown below in Figure 2 for a case where the storage pressure ratio of $\frac{p_{Ao}}{p_{Bo}} = 200$. The subscripts Ao and Bo refer to the initial states of the hydrogen and air respectively. In this case, the most reactive mixture of the two gasses is found when z=0.0065.

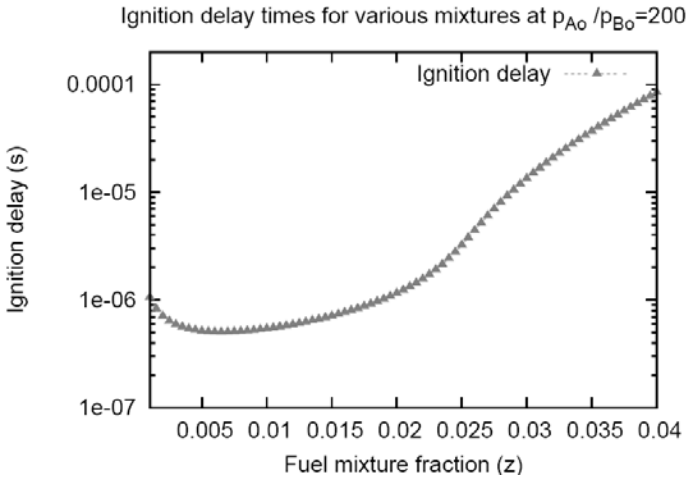

Figure 2. Ignition delay times for various mixture fractions of fuel to air for a case where $\frac{p_{Ao}}{p_{Bo}} = 200$.

2.6 Validation of the 1-D Lagrangian Reaction-Diffusion Model

To validate the code, flame speed calculations were performed for an unsteady laminar premixed hydrogen flame at constant pressure. The flame speed is obtained for a stoichiometric mixture of hydrogen and air at 1 atm and 300K. The result is compared against the flame speed obtained using Cantera's built in steady flow solver using mixture-averaged transport properties. The Cantera simulation is able to compute a steady solution with its finest grid resolved at $\Delta x = 8.0 \times 10^{-6} m$. Applying the transformation given in equation (3) at the minimum density gives us the corresponding resolution in Lagrangian coordinates: $\Delta m = 2.64 \times 10^{-6} kg/m^2$. The comparison between the two models is shown below in Figure 4. The *Lagrangian reaction-diffusion model* was found to have a higher flame speed value than that calculated by Cantera. The reason for this is because the Cantera flame solver does not include the energy addition term, $\rho^2 \frac{\partial \mathrm{T}}{\partial \mathrm{m}} \sum_{i=1}^{N} Y_i C_{p,i} v_{d,i}$, found in equations (2) and (5). When this term was neglected in the Lagrangian model, the flame speed was found to converge to the same flame speed calculated with Cantera, which was 2.4 m/s. Therefore, the model

is considered to be in good agreement with Cantera's solver and is therefore considered to provide good results for the numerical experiments conducted in this study.

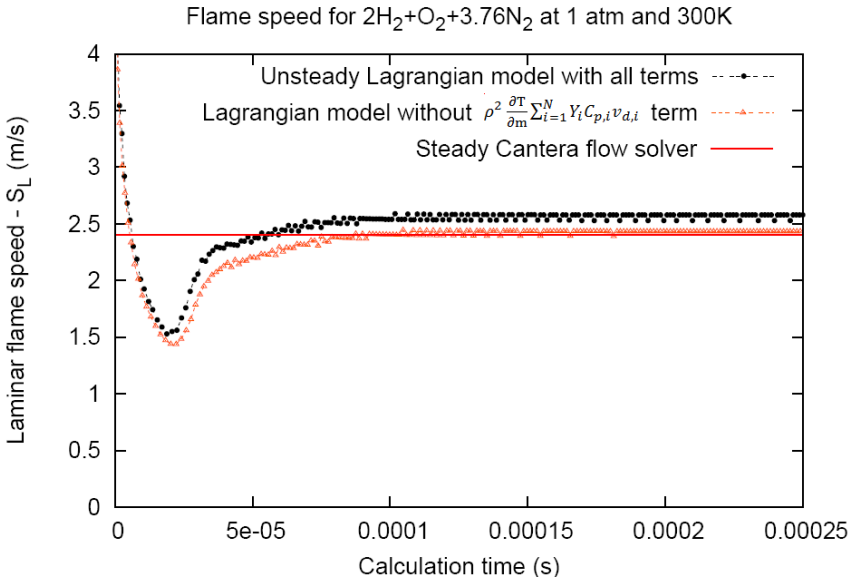

Figure 4. Flame speed calculation for a premixed stoichiometric mixture of hydrogen and air at 1 atm and 300K.

3.0 RESULTS AND DISCUSSION

Various jets with pressure ratios ranging from $\frac{p_{Ao}}{p_{Bo}} = 75$ to 800 were simulated with varying hole sizes in order to determine the critical point, or hole size, at which ignition is quenched. Temperature and OH mass fraction profiles are shown below in Figures 5 and 6, respectively, for a case where $\frac{p_{Ao}}{p_{Bo}} = 300$ with the *Lagrangian reaction-diffusion model*. Results indicate that for large hole sizes, ignition occurs as it would if there were no expansion. As the hole size is reduced, the onset of pressure decay occurs sooner causing a cooling effect in the gas. Despite this cooling effect, however, it is still possible for chemical reactions to occur which can lead to ignition. With a further reduction in hole size, a critical point is reached where ignition is not observed. Although there are still chemical reactions that occur on very small scales at the critical point, they do not contribute to any significant large scale changes in the temperature or composition of the gas. Furthermore, the critical point at which the ignition occurs is very sensitive to small changes in the hole size. The smallest change in hole size can lead to full blown ignition, or no ignition at all. This reflects the strong competition between chemical reactions and expansion at this point. For the purpose of this study, a successful ignition event occurs when the OH mass fraction at any given point exceeds 0.001. The simulation, shown in Figures 5 through 10, was conducted on a domain that consists of 500 grid points with a resolution of $\Delta m = 2.0 \times 10^{-7} kg/m^2$. It is important to note that the domain must be large enough to capture the ignition phenomena. In this case, the domain must start at least $5 \times 10^{-5} m$ from the contact surface on the hot air side in order to properly capture ignition.

Figures 7 through 10 show the profiles for H2, O2, N2 and H2O, respectively. When no expansion is prescribed, ignition is always observed. The two gasses diffuse into each other. As the two gases mix, H2 and O2 are consumed by chemical reactions and H2O is eventually produced. Heat is released during the process and ignition is observed on the hot air side, which can be reflected by the 'hump' in temperature profile in Figure 5. For the super-critical case we can see that there is an initial drop in temperature as the gases expand. However, once the OH mass fractions increase above approximately 0.001, the chemical reactions accelerate and eventually there is an increase in temperature, and thus ignition occurs. For the sub-critical case, OH mass fraction peaks at 1×10^{-6} seconds and then becomes smaller as the reaction progresses in time. Therefore the reaction is quenched and no increase in temperature is observed.

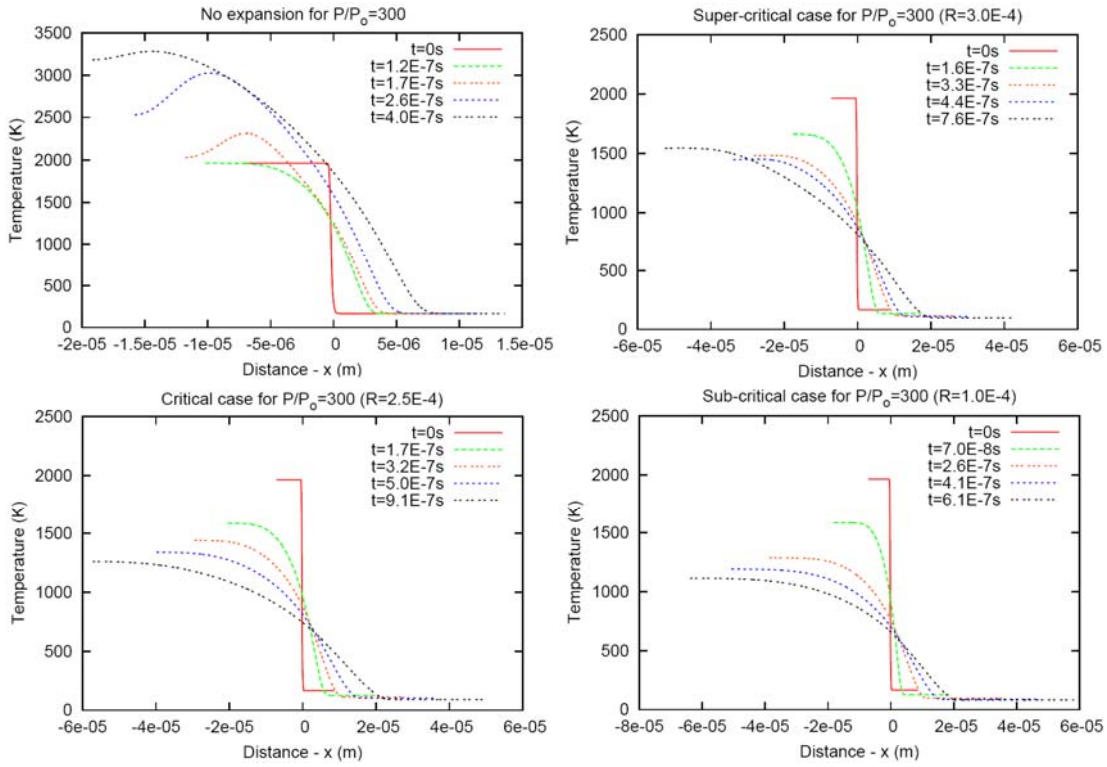

Figure 5. Temperature profiles for 4 cases: 1) no expansion, 2) super-critical case, 3) critical case, and 4) sub-critical case.

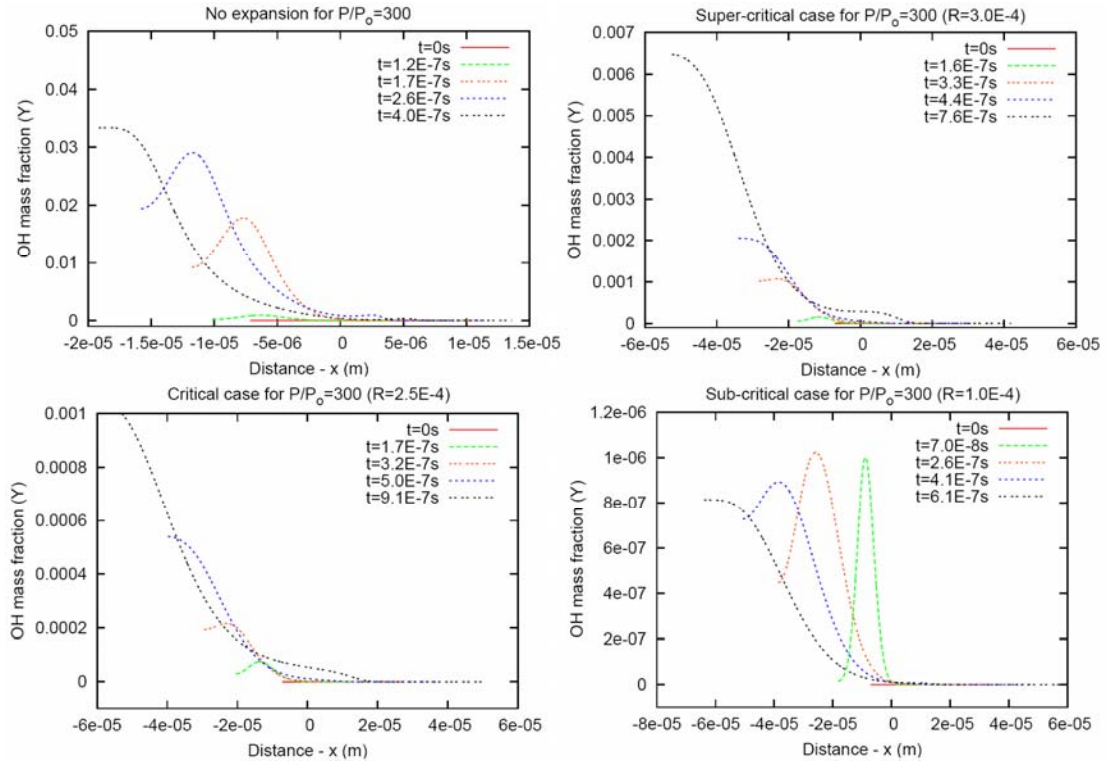

Figure 6. OH mass fraction profiles for 4 cases: 1) no expansion, 2) super-critical case, 3) critical case, and 4) sub-critical case.

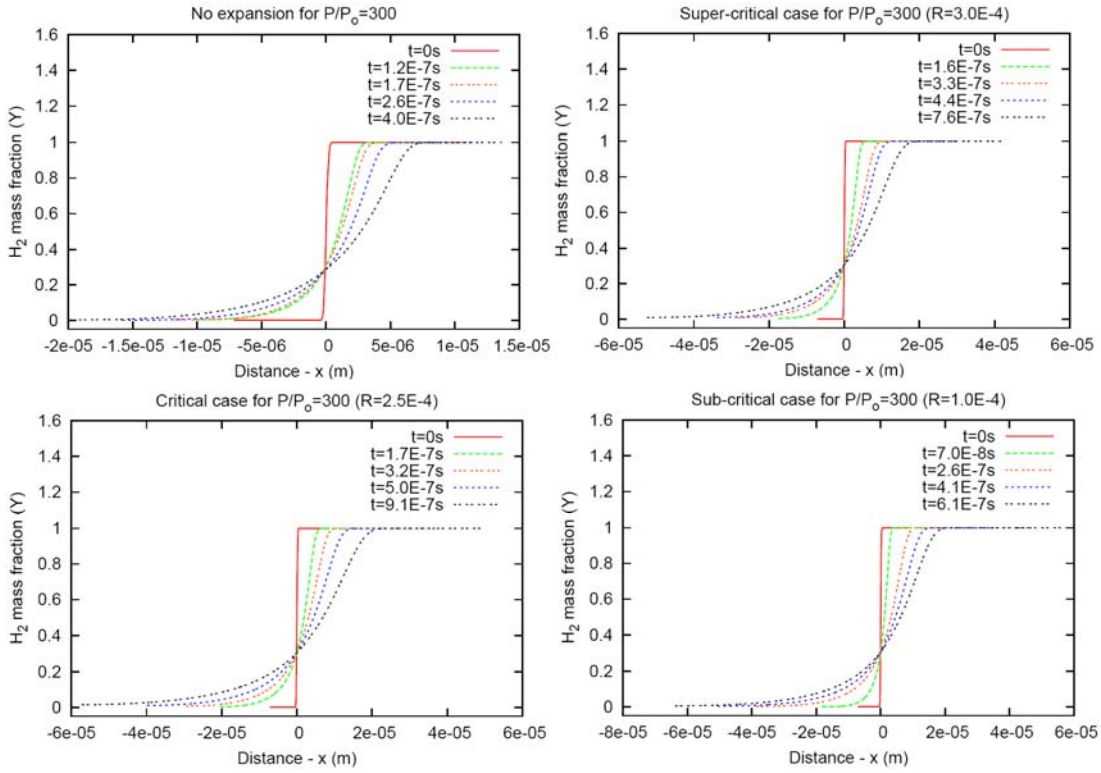

Figure 7. H2 mass fraction profiles for 4 cases: 1) no expansion, 2) super-critical case, 3) critical case, and 4) sub-critical case.

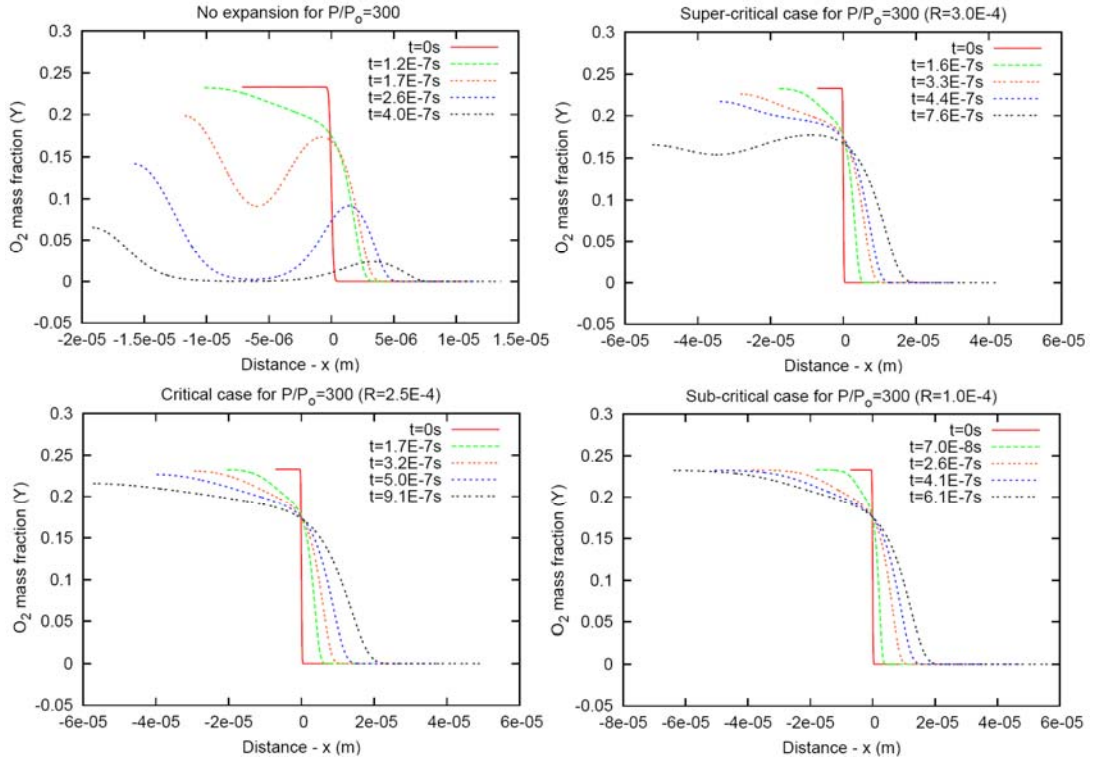

Figure 8. O2 mass fraction profiles for 4 cases: 1) no expansion, 2) super-critical case, 3) critical case, and 4) sub-critical case.

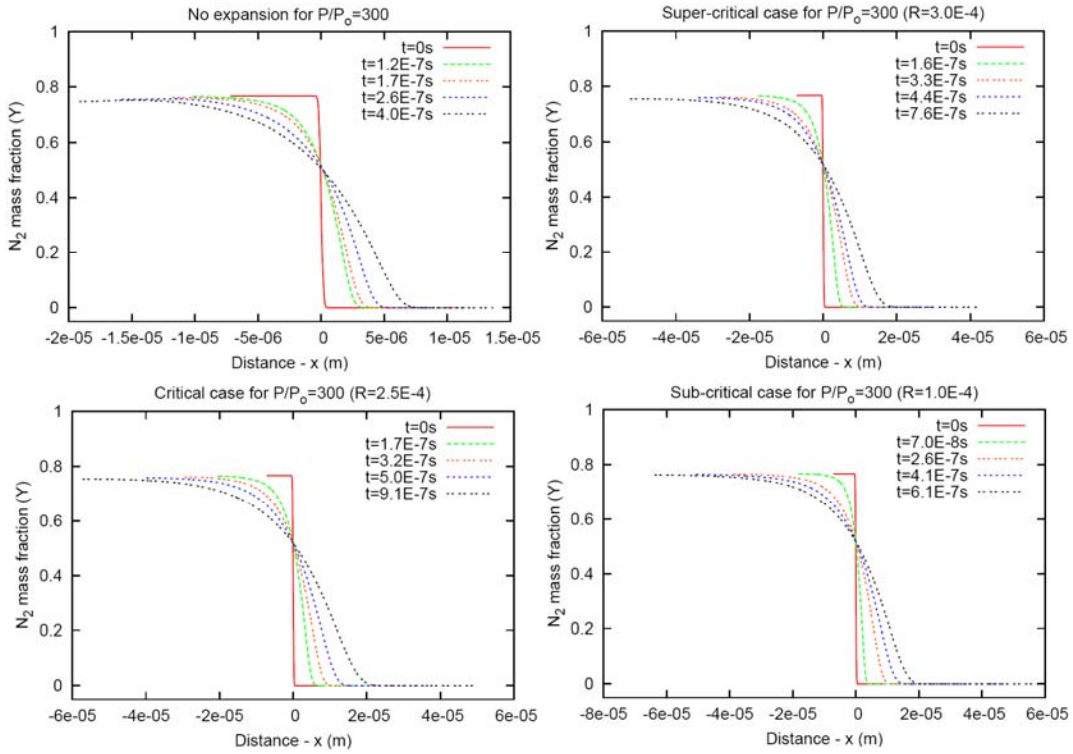

Figure 9. N2 mass fraction profiles for 4 cases: 1) no expansion, 2) super-critical case, 3) critical case, and 4) sub-critical case.

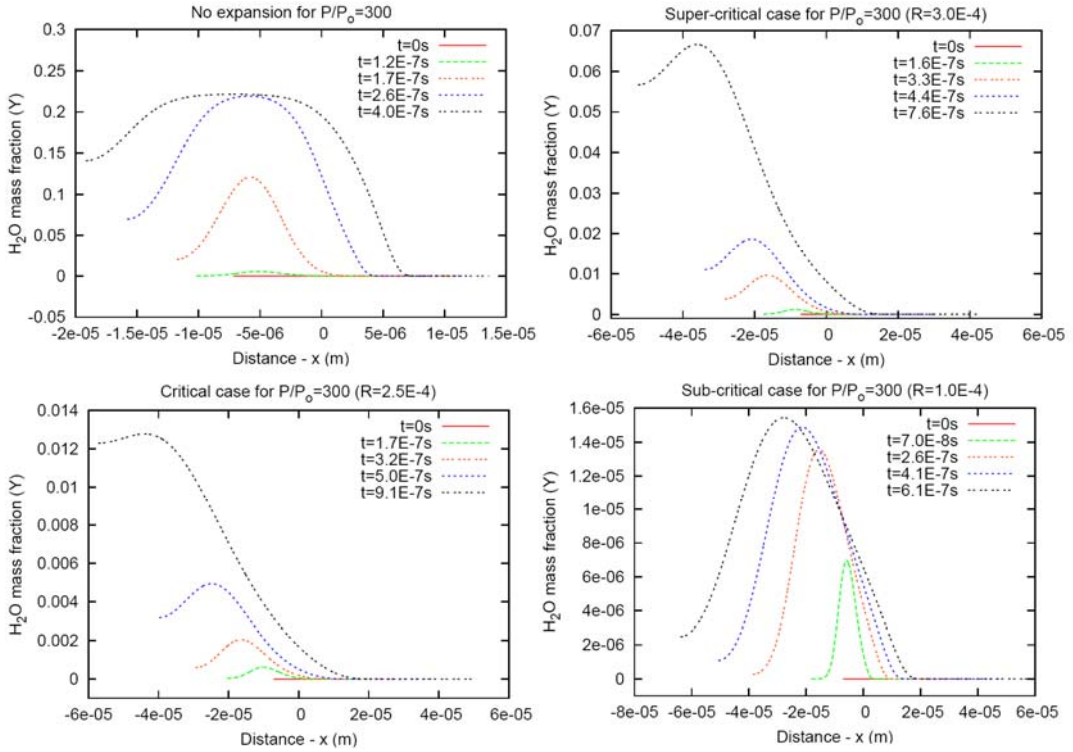

Figure 10. H2O mass fraction profiles for 4 cases: 1) no expansion, 2) super-critical case, 3) critical case, and 4) sub-critical case.

The critical hole size for which the onset of ignition occurs for various pressure ratios is shown below in Figure 7. The critical hole size is shown for both the *Lagrangian reaction-diffusion model* and the *homogeneous mixing ignition model*. The critical hole sizes were determined based on the ignition criteria of OH mass fractions described above. It is clear from the figure that higher storage pressures of hydrogen require smaller holes for the gas to escape through in order for ignition to be quenched. If the storage pressure and hole size corresponds to a location that is to the lower left of the curve, ignition is quenched. If the storage pressure and hole size lies to the upper right of the curve ignition is observed. Experimentally, Golub's group [2] had conducted lab experiments for hole diameters of 5mm. The critical point of ignition observed by Golub's group is shown in the figure. Comparing the experimental results to the numerical results in Figure 3 proved to be in good agreement.

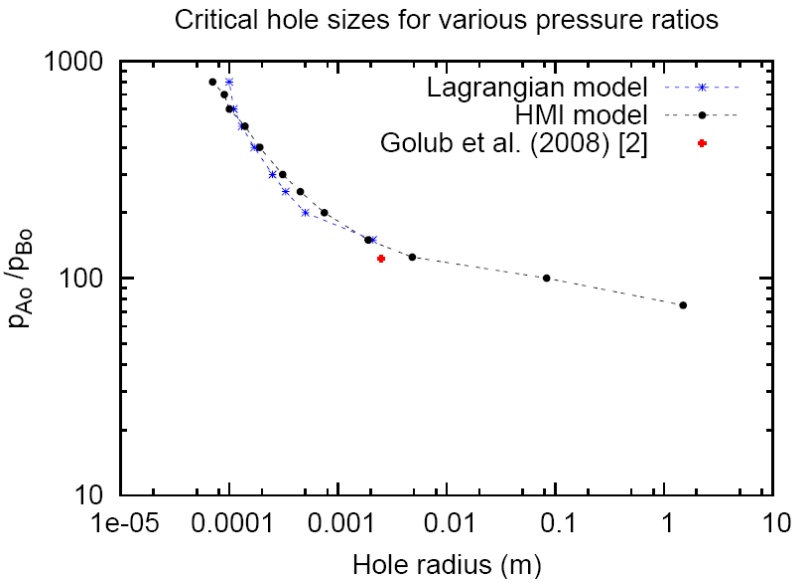

Figure 7. Critical hole sizes to quench ignition at various pressure ratios, $\frac{p_{Ao}}{p_{Bo}}$.

One final observation that is made from Figure 7 is that there is a significant change in the slopes of both curves around a storage pressure of $\frac{p_{Ao}}{p_{Bo}} = 150$. Below this storage pressure, the ignition is severely inhibited due to the well-known cross-over effect in hydrogen ignition [9]. For a storage pressure of 150 atm, the temperature and pressure at the interface reach 1500 K and 28 atm. At temperatures and pressures below this limit, the chain branching reactions are inhibited by rapid chain termination reactions. For all practical purposes, ignition becomes very difficult below this critical limit.

4.0 CONCLUDING REMARKS

The results of the simulations indicate that for every storage pressure, there exists a critical hole size below which ignition is prevented during the release process. Close inspection of the results indicate that this limit is due to the competition between the heating provided by the shock wave and the cooling due to expansion. In particular, the storage pressure controls the strength of the shock that is observed upon release which in turn controls the temperature and pressure of the gases behind the shock. Also, the size of the opening determines the rate at which the mixing layer expands, or cools. This cooling effect was found to be more efficient for smaller holes. Smaller holes experienced more rapid depressurization, and thus require a higher storage pressure in order for ignition to occur. Furthermore, the results also indicate that the details of the mixing process do not play a significant role to leading order. The limiting ignition criteria were found to be well approximated by the Homogeneous Ignition Model of Cuenot and Poinsot, which was supplemented by a heat loss term due

to expansion. Therefore, turbulent mixing occurring in reality is not likely to affect the ignition limits derived in the present study. Comparison with existing experiments also showed very good agreement. These results have significance in terms of generating the appropriate codes and standards regarding the storage and handling of hydrogen.

REFERENCES

1. Dryer, F.L., Chaos, M., Zhao, Z., Stein, J.N., Alpert, J.Y. and Homer, C.J., Spontaneous ignition of pressurized releases of hydrogen and natural gas into air, *Combust. Sci. Tech.* **179**, 2007, pp. 663-694.
2. Golub, V.V., Baklanov, D.I., Golovastov, S.V., Ivanov, M.F., Laskin, I.N., Saveliev, A.S., Semin, N.V. and Volodin V.V., Mechanisms of high-pressure hydrogen gas self-ignition in tubes, *Journal of Loss Prevention in the Process Industries*, **21**, 2008, pp. 185-198.
3. Mogi, T., Kim, D., Shiina, H. and Horiguchi, S., Self-ignition and explosion during discharge of high-pressure hydrogen, *Journal of Loss Prevention in the Process Industries*, **21**, 2008, pp. 199-204.
4. Wolanski, P. and Wojcicki, S., Investigation into the mechanism of diffusion ignition of a combustible gas flowing into an oxidizing atmosphere, 14th Symp. (Int.) on Combustion, Pittsburgh, PA, The Combustion Inst., 1973, pp. 1217-23.
5. Liu, Y.F., Tsuboi, N., Sato, H., Higashino, F. and Hayashi, A.K., Direct numerical simulation on hydrogen fuel jetting from high pressure tank, 20th Intl Colloquium on the Dynamics of Explosions and Reactive Systems, July 31-August 5, 2005, McGill University, Montreal, Canada.
6. Xu, B.P., Hima, L.E., Wen, J.X., Dembele, S., Tam, V.H.Y. and Donchev, T., Numerical study on the spontaneous ignition of pressurized hydrogen release through a tube into air, *Journal of Loss Prevention in the Process Industries*, **21**, 2008, pp. 205-213.
7. AMRITA, 2009, available from http://www.amrita-cfd.org/
8. Rogg, B. and Wang, W., Run-1DL user manual, Lehrstuhl fur Stromungsmechanik, Institut fur Thermo-und Fluiddynamik, Ruhr-Universitat Bochum, D-44780 Bochum Germany, 1995.
9. Law, C. K., Combustion Physics, 2006, Cambridge University Press, New York.
10. Cantera, 2008, available from http://www.cantera.org/ or http://sourceforge.net/projects/cantera
11. Li, J., Zhao, Z., Kazakov, A. and Dryer, F.L., An updated comprehensive kinetic model of hydrogen combustion, *International journal of chemical kinetics*, **36**, No. 10, 2004, pp. 566-575.
12. SUNDIALS, 2008, available from https://computation.llnl.gov/casc/sundials/main.html
13. Kee, R.J., Rupley, F.M., Miller, J.A., Coltrin, M.E., Grcar, J.F., Meeks, E., Moffat, H.K., Lutz, A.E., Dixon-Lewis, G., Smooke, M.D., Warrantz, J., Evans, G.H., Larson, R.S., Mitchell, R.E., Petzold, L.R., Reynolds, W.C., Caracotsios, M., Stewart, W.E., Glarborg, P., Wang, C. And Adigun, O., Chemikin collection release 3.6, Reaction Design Inc., San Diego, CA, 2000.
14. Knikker, R., Dauptain, A., Cuenot, B. and Poinsot, T., Comparison of computational methodologies for ignition of diffusion layers, *Combustion Science and Tec*hnology, **175**, No. 10, 2003, pp. 1783-1806.
15. Liepmann, H.W. and Rhoshko, A., Elements of Gas Dynamics, 2001, Dover.
16. Browne, S., Ziegler, J. and Shepherd, J.E., Numerical solution methods for shock and detonation jump conditions, California Institute of Technology: Aeronautics and Mechanical Engineering (GALCIT Report FM2006.006), 2008.
17. Radulescu, M.I. and Law, C.K., The transient start of supersonic jets, *J. Fluid Mech*, **578**, 2007, pp. 331-369.